Technical Report

Analysis of $\bar{p}p \longrightarrow 0^-\omega$ in flight

Karsten Beuchert, Ruhr-Universität Bochum
e-mail: karsten.beuchert@zentrale.adac.de

Abstract

In order to analyze complicated decay channels of the proton antiproton system in flight it is useful if not necessary to know the contributing initial angular momentum states. Since complicated decay channels contain a lot of not or badly known parameters (such as resonance masses and widths e.g.) an estimate of the contributing initial states may be obtained by investigating relatively simple and non-resonant (no intermediate resonance from a production process) final states and determining their contributing angular momenta. This report is to present the selections and partial wave analyses of reactions of the type $\bar{p}p \longrightarrow 0^-\omega$ ($0^- = \pi^0,\eta,\eta'$) for incident antiproton momenta of 0.6, 1.2 and 1.94 GeV/c on a fixed liquid hydrogen target.
The highest contributing angular momenta found in these analyses are:

- 600 MeV/c: $J_{max} = 3\ \hbar$
- 1200 MeV/c: $J_{max} = 4\ \hbar$
- 1940 MeV/c: $J_{max} = 5\ \hbar$

Contents

Chapter 1

Basic software

Standard CERN and CB software were used as basis for the programs and algorithms used for selection, reconstruction and analysis of the data.
For the selection and reconstruction standard CB software was applied: CBOFF 1.25/02 [12], BCTRAK 2.01/00 with the PDRGBC algorithm [13], LOCATER 1.93/03 [18], GTRACK 1.32/00 [8], CBKFIT 3.00/03 [14]. The channel specific routines were written using standard "C" routines from the "C" library CBoOFF [3].
For the Monte Carlo simulation of $\bar{p}p$ reactions CBGEANT 4.06/07 [20] basing on GEANT 3.15/90 [6] was used.
Visualization, n-tuple handling and histogram operations were done using CERN packages HBOOK [1] and PAW [7].
The development of the fit routines was based on CERN program MINUIT [2] using the MIGRAD method.

Chapter 2

Reconstruction and selection

2.1 Data samples

The data used for these analyses mainly consisted of events which had been taken with an on-line 0-prong trigger. This means that neither hits in the PWC's nor in the innermost three layers of the JDC had been allowed to occur, in addition to the usual minimum bias trigger conditions ensuring a real antiproton proton reaction (signal from the entrance counters and no signal from the veto counter). Additionally, a minimal value for the fast FERA energy sum was required. The term *all neutral trigger* will be used synonymously for these data.
The data statistics concerning 1940 MeV/c were improved by adding the all neutral part of data taken in August 1994 with a so called *mixed trigger* which was intended to enrich 0-prong and 2-prong events at the same time.
The data from all available run periods were summed up in order to achieve sufficient statistics. The definition of pile up events depends on the veto counter used and on the trigger configurations. They were different during several run periods. Consequently a rejection of pile up events will make the data samples inconsistent. Pile up events probably will show up with enlarged particle multiplicities and energy and will be rejected by the analysis. Therefore pile up events were allowed for the analysis.
The statistics used are shown in table 2.1.

2.2 Event reconstruction

Only the neutral electromagnetic decay modes of the mesons are considered. With the two photon decay of the pseudoscalar mesons ($0^- = \pi^0, \eta, \eta'$) $0^- \longrightarrow \gamma\gamma$ and the decay of the ω meson $\omega \longrightarrow \pi^0\gamma$ the decay chain

$$\bar{p}p \longrightarrow 0^-\omega \longrightarrow 0^-\pi^0\gamma \longrightarrow 5\gamma$$

results in a five photon final state and contains the three channels

- $\bar{p}p \longrightarrow \pi^0\omega$
- $\bar{p}p \longrightarrow \eta\omega$
- $\bar{p}p \longrightarrow \eta'\omega$

beam momentum [MeV/c]	beam period	trigger	# of events in total	# of events only neutrals
600	April/May 1993	0 prong	2 801 862	2 266 054
1200	December 1991	0 prong	1 574 307	1 502 350
	July 1992	0 prong	1 409 025	1 321 896
	April/May 1993	0 prong	8 690 455	7 315 274
	August 1994	0 prong	1 414 995	1 081 728
		Σ	13 088 782	11 221 048
1940	July 1992	0 prong	6 945 965	5 590 895
	August 1994	0 prong	3 263 167	2 527 387
	August 1994	mixed	440 695	440 695
		Σ	10 649 827	8 558 977

Table 2.1: *Data used for selection. The entry for the total number of events of the "mixed" trigger refers to the number of neutral events extracted off-line and therefore is identical to the entry in the "neutrals" column.*

When traversing the crystals of the barrel each of these photons deposits most of its energy and thus gives rise to a local energy maximum in the barrel. In the following such a local maximum will be called PED (Particle Energy Deposit). In the simplest case there is a unique relation between a photon and a PED. Therefore most of the reactions of the desired type will show up as 5 PED events. Unfortunally there are some processes which cause a difference between the number of PEDs found and the number of photons created during the reaction chain. The ones most important for an all neutral analysis are:

- an increase of the number of PEDs may be produced by
  - noise
  - electromagnetic shower fluctuations (fig. 2.1.a)
- a decrease of the number of PEDs may be caused by
  - particle loss
  - high energetic mesons (especially so called "merging pions") (fig. 2.1.b)

The problems of charged tracks depositing energy in the crystals and of hadronic shower fluctuations may be neglected for these analyses since in addition to the on-line cut in a first step all remaining events with charged tracks are rejected.

2.2.1 Handling of noise

For the reduction of the influence of noise BCTRAK standard parameters were used. The values of these parameters were set to:

- ECLSBC = 4 MeV (standard value)
- EXTLBC = 1 MeV (standard value)
- ECLUBC = 10 MeV
- EPEDBC = 10 MeV

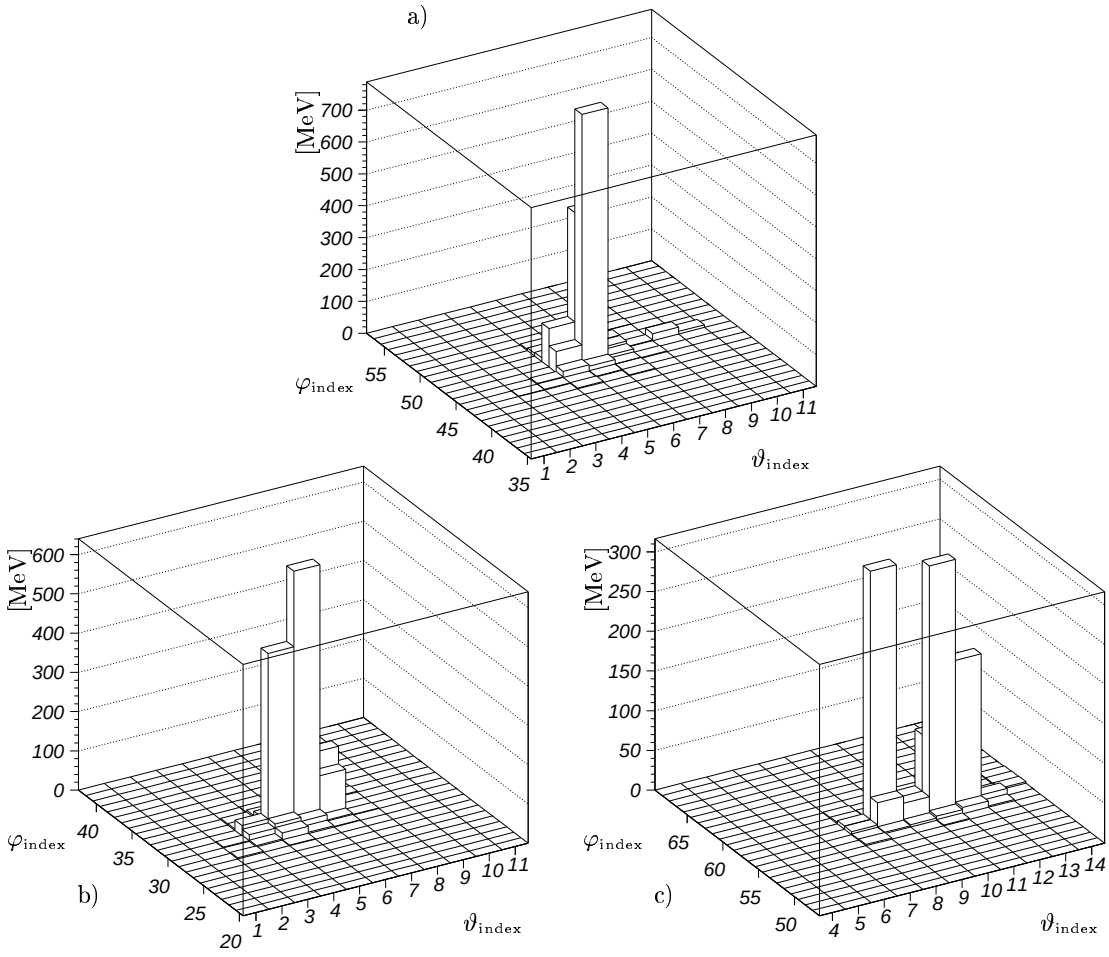

Figure 2.1: *Energy distribution in Monte Carlo simulated clusters of different origins. The x axes mean the ϑ index of the crystal layers, the y axes mean the φ index. The z axes mean the energy deposit in the crystal. Each plot is centered around the crystal with the highest energy deposit (central crystal). Fig. a) shows a cluster, which was produced by a photon. In crystal layer no. 9 one can see an electromagnetic split off (from $\bar{p}p \longrightarrow \gamma\gamma$ at 1940 MeV/c). Fig. b) shows a cluster which was produced by the two photons from a π^0 decay but gives rise to only one PED (from $\bar{p}p \longrightarrow \pi^0\gamma$ at 1940 MeV/c). Fig. c) shows a cluster which was produced by a π^0 and consists of two PEDs (from $\bar{p}p \longrightarrow \pi^0\pi^0$ at 1940 MeV/c).*

The values for ECLUBC and EPEDBC were chosen lower than the standard value which makes an explicit handling of electromagnetic shower fluctions (in the following: split offs) possible and necessary.

2.2.2 Handling of split offs

Split offs arise from statistical fluctuations during the development of an electromagnetic shower and show up as (in most cases low energetic) local energy maxima in a cluster. In order to reconstruct the events correctly those split offs have to be distinguished from PEDs caused by low energy photons.
This work is done by the artificial neural feed forward network developed by Thomas Degener [11].

2.2.3 Particle loss

The Crystal Barrel detector exhibits a symmetry appropriate for collider mode. Due to the hole in forward direction this implies large acceptance losses for the actual fixed target mode when considering annihilation in flight.
In priciple one can try to recover uncomplete events by means of missing particle techniques as has been done before with Crystal Barrel data at rest. After careful studies of this sub data sample it turned out that for annihilation in flight missing particle techniques are more difficult, so that the use of them is not worth the effort. Partly this is due to the PED energy correction which worked better for the typical energies occuring at rest than for the energies connected with annihilation in flight. Another point is the position of the vertex which is better known for annihilation at rest than for annihilation in flight in which the annihilation may have happened at any z coordinate of the target with almost equal probability.
Quite a principal problem for any missing particle analysis is the fact that most of the all neutral data have been taken with an on-line cut on the total event energy. This means that the events needed for a missing particle analysis do not even exist within these data samples. Therefore one has to use minimum bias data from which one obtains only very poor statistics for the channels of interest.

2.2.4 Merging pions

The angle between the photons from a mesonic decay as seen in the laboratory system (detector) depends on the angle between one of the photons and the direction of motion of the meson as seen in the CM-System and on its energy. In the simplest case the energy deposits of the two photons from one decay are well separated in the barrel. Even for annihilation at rest one observes clusters with two PEDs arising from the two photons from one decay. The minimal possible opening angle between the two decay photons decreases with increasing meson energy and therefore with increasing beam momentum (table 2.2). For annihilation in flight the opening angle between the two decay photons may get too small for the calorimeter to resolve. In that case the total energy deposit from both decay photons (which means: from the meson) looks as if it arised from one photon (fig. 2.1.b). In order to save events with merged pions for the analysis these PEDs have to be distinguished from photonic PEDs. From earlier analyses at rest it has been known that there is a quantity, called *shower mass*, which according to its definition is an approximate measurement for the mass of the particle causing a cluster. For the two-PED-clusters of pionic origin occuring at rest this quantity shows a clear peak near the pion mass.
For annihilation in flight mesons with higher energy occur. There are some interesting things to observe. At high energies η mesons start to produce clusters with two PEDs which, analogously, show shower masses near the mass of the eta meson. Another observation is that the shower mass depends, in contrast to the physical rest mass, on the meson

decay of the	π^0 meson			
beam momentum [MeV/c]	at rest	600	1200	1940
$\bar{p}p \longrightarrow \pi^0\omega$	19.93	13.86	9.74	6.87
$\bar{p}p \longrightarrow \pi^0\omega$, π^0 from $\omega \longrightarrow \pi^0\gamma$	16.56	11.72	8.48	6.17
$\bar{p}p \longrightarrow \eta\omega$, $\omega \longrightarrow \pi^0\gamma$	18.39	12.87	9.14	6.52
$\bar{p}p \longrightarrow \eta'\omega$, $\omega \longrightarrow \pi^0\gamma$	25.52	16.86	11.12	7.51

decay of the	η meson				η' meson			
beam momentum [MeV/c]	at rest	600	1200	1940	at rest	600	1200	1940
$\bar{p}p \longrightarrow \eta\omega$, $\omega \longrightarrow \pi^0\gamma$	79.60	56.21	39.60	27.93	-	-	-	-
$\bar{p}p \longrightarrow \eta'\omega$, $\omega \longrightarrow \pi^0\gamma$	-	-	-	-	139.83	100.50	70.31	49.28

Table 2.2: *Minimal possible opening angles (in °) in the laboratory system for two photon decays of pseudoscalar mesons from channels of the type $0^-\omega$. The given values refer to the nominal masses of the considered particles [19]. For the channel $\pi^0\omega$ the most energetic pions stem from the decay $\omega \longrightarrow \pi^0\gamma$.*

energy and its polar angle. The angular dependence is negligible in comparison with the energy dependence and will not be considered in the following. A very interesting point is that this behaviour may be generalized to clusters of arbitrary PED multiplicity, only provided that the cluster is produced by one single particle. In this context a cluster produced by both photons from a mesonic decay ($M \longrightarrow \gamma\gamma$) is considered as being produced by the meson.
In order to distinguish clusters of different origin (mesonic or photonic) the energy depence of the shower mass has to be parametrized. For this purpose different Monte Carlo data of channels typical for $\bar{p}p$ annihilation have been produced with different beam momenta. From these data pure mesonic clusters (π^0 or η) were extracted according to the following criteria:

- every daughter particle from the mesonic decay chain which was created before hitting the crystals has deposited its energy in the same cluster,
- the cluster does not contain any energy from decay chains of other particles,
- at least 75% of the mesonic energy has been deposited in total.

The considered energy region was divided into intervals of 100 MeV. Connected with each interval is a distribution of the shower mass μ with a specific mean value $\bar{\mu}$ and width σ. These shower mass distributions were fitted with Gaussians yielding one value for the mean and one value for the width per interval. The resulting distributions of mean and width were used in order to describe the energy dependence of the mesonic shower mass (fig. 2.2).
It turned out that using only Monte Carlo simulations of channels observed with Crystal Barrel up to a beam momentum of 1940 MeV/c was not sufficient to stabilize this parametrization at the end points. Therefore CBGEANT was used in order to produce one pion events with different energies up to the limits of the readout electronics. From these events again purely mesonic clusters were extracted. Adding these artificial data to the existing Monte Carlo data sample successfully stabilized the parametrization.
Be $E\,[GeV]$ the energy of the cluster (after running standard CBOFF). Then the parametrization obtained for pionic clusters reads:

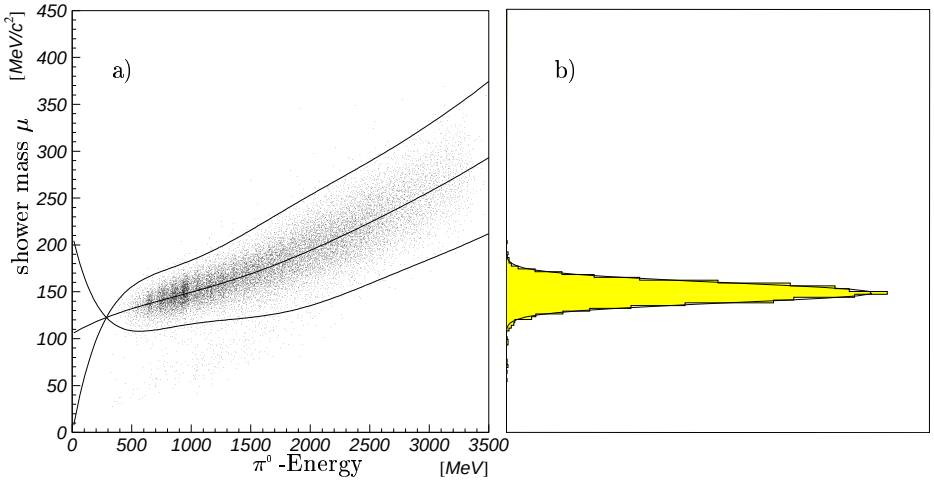

Figure 2.2: *Energy dependence of the shower mass. The data points in a) fulfill the requirements for purely pionic clusters. For a beam momentum of 1940 MeV/c pions occur with energies up to 2500 MeV. The solid line shows the parametrization of the distribution (mean and 3σ bands). There are no pionic clusters below the crossing point of the curves. As an example fig. b) shows the projection onto the shower mass axis for the energy interval between 900 MeV and 1000 MeV and the fitting Gaussian.*

$$\begin{aligned}\mu_{\text{shower mass}}\left[GeV/c^2\right] &= 105.16 \\ &+ 0.74907 \cdot 10^{-1} \cdot E \\ &- 0.59117 \cdot 10^{-4} \cdot E^2 \\ &+ 0.37134 \cdot 10^{-7} \cdot E^3 \\ &- 0.93325 \cdot 10^{-11} \cdot E^4 \\ &+ 0.87289 \cdot 10^{-15} \cdot E^5 \end{aligned} \tag{2.1}$$

$$\begin{aligned}\sigma_{\text{shower mass}}\left[GeV/c^2\right] &= -35.298 \\ &+ 0.20787 \cdot E \\ &- 0.38871 \cdot 10^{-3} \cdot E^2 \\ &+ 0.37826 \cdot 10^{-6} \cdot E^3 \\ &- 0.20240 \cdot 10^{-9} \cdot E^4 \\ &+ 0.60470 \cdot 10^{-13} \cdot E^5 \\ &- 0.94767 \cdot 10^{-17} \cdot E^6 \\ &+ 0.60803 \cdot 10^{-21} \cdot E^7 \end{aligned} \tag{2.2}$$

There is a point at the low energetic end of this distribution where the widths become negative. This is acceptable since below this point pionic clusters do not occur.
The energy dependence of shower masses produced by η mesons becomes important only when dealing with beam momenta higher than achievable with LEAR. For all beam momenta below 2000 MeV/c it turned out to be sufficient to use a simple shower mass window with a mean value of 557.98 MeV/c^2 and a width of 29 MeV/c^2.

	beam momentum [MeV/c]	600	1200	1940
	# of neutral events	2 266 054	10 923 847	8 558 977
general selection	cuts on multiplicities			
	1. PED-multiplicity ($4 \leq \#_{\mathrm{PEDs}} \leq 10$)	1 608 966	8 431 557	6 044 919
	2. π^0 - and η-multiplicities	1 603 230	8 315 659	5 916 326
	3. γ-multiplicity (neural network)	250 224	1 222 317	839 153
	kinematic fit			
	4. final state (5γ or $\pi^0\gamma\gamma\gamma$)	75 121	381 910	181 858
	5. $\pi^0 0^-\gamma$ ($0^- = \pi^0$, η or η')	59 146	327 784	160 049
	6. $\omega\gamma\gamma$	33 515	170 466	73 710
	7. vertex	31 920	163 245	63 790
channel specific selection	8. $\bar{p}p \longrightarrow \pi^0\omega$			
	a. consistency of $\pi^0\pi^0\gamma$ and $\omega\gamma\gamma$	12 486	64 716	28 485
	b. consistency with meson recognition	12 462	64 340	27 989
	c. no shower fluctuation (5 PEDs at most)	8 183	41 663	17 320
	9. $\bar{p}p \longrightarrow \eta\omega$			
	a. consistency of $\pi^0\eta\gamma$ and $\omega\gamma\gamma$	5 421	20 029	7 051
	b. consistency with meson recognition	4 875	17 667	6 102
	c. no shower fluctuation (5 PEDs at most)	3 269	11 283	3 660
	d. no merged π^0 ("'1-PED-π^0"')	3 269	11 222	3 434
	e. cut on ω decay angle	2 880	9 732	3 032
	10. $\bar{p}p \longrightarrow \eta'\omega$			
	a. consistency of $\pi^0\eta'\gamma$ and $\omega\gamma\gamma$	1 964	too low statistics	
	b. consistency with meson recognition	670	with too large	
	c. no shower fluctuation (5 PEDs at most)	393	background	
	d. no merged π^0 ("'1-PED-π^0"')	393		
	survey of selected statistics			
	$\bar{p}p \longrightarrow \pi^0\omega$ (4 & 5 PEDs)	8 183	41 663	17 320
	5 PEDs	8 181	40 898	14 263
	4 PEDs	2	765	3 057
	$\bar{p}p \longrightarrow \eta\omega$ (5 PEDs)	2 880	9 732	3 032
	$\bar{p}p \longrightarrow \eta'\omega$ (5 PEDs)	393	too low statistics	

Table 2.3: *Steps of selection and results for the $0^-\omega$ selections. Detailed explanations are given in the text.*

2.2.5 Photons

Every PED which is not suppressed due to noise reduction and which is neither recognized as split off nor as merging pion is regarded as a photon.
For annihilation at rest often PEDs with their central crystal in layer 13 have been rejected since due to the expected lateral energy losses an energy correction is more difficult than for the other crystals. For annihilation in flight this cut becomes fatal since it drastically enlarges the regions of bad or even vanishing detector acceptance near the beam axis. Therefore this cut is not applied. Since the kinematic fit is very sensitive to the total event energy badly measured events are rejected by the fit anyway (cf. table 2.3, step 4).

2.2.6 Event reconstruction

Preselection

The analysis was based only on completely detected events. That means, that events with missing particles were not taken into account. The completely detected events may consist of

- photonic PEDs
- pionic PEDs
- shower fluctuation PEDs.

Up to a beam momentum of 1940 MeV/c there is not enough energy to boost both pions from the decay chain $\bar{p}p \longrightarrow \pi^0\omega \longrightarrow \pi^0\pi^0\gamma$ sufficiently to make each of them merge to one PED. Therefore only one merged pion per event was permitted making four the lowest allowed PED multiplicity (cf. table 2.3, step 1). Nevertheless the energy is sufficient for all occuring pions and η mesons to produce a 2-PED-cluster. These clusters may be recognized by the method described above. An event of the type $0^-\omega$ may at most show two pions *or* one pion and one η meson. Events with higher mesonic multiplicities were rejected before applying the neural network (table 2.3, step 2).
The number of shower fluctuation PEDs is arbitrary. In order to save as many events as possible for the analysis in a first step events with up to five additional PEDs were allowed (table 2.3, step 1). The purity of the data was improved using an artificial neural network in order to distinguish shower fluctuations from real photons (table 2.3, step 3). It turned out that due to the much higher frequency of annihilation events with higher photon multiplicity there was still a large background within the data samples of events with shower fluctuations. Therefore these events were rejected in a later step (table 2.3, steps 8.c, 9.c, 10.c).

Kinematic fit

There were three different types of event signatures which the kinematic fit had to be applied on:

1. $\bar{p}p \longrightarrow 0^-\omega \longrightarrow \gamma\gamma\gamma\gamma\gamma$
2. $\bar{p}p \longrightarrow 0^-\omega$, $0^- \longrightarrow \gamma\gamma$, $\omega \longrightarrow \pi^0\gamma$, π^0 from ω detected as 1 PED,
3. $\bar{p}p \longrightarrow \pi^0\omega$, $\omega \longrightarrow \gamma\gamma\gamma$, π^0 recoiling against ω detected as 1 PED.

The algorithm for putting the merged pions into the global tracking bank was adopted from PI0FND [21]. All events were fitted with a free vertex. In order to reject bad events a probability cut at 1% was applied, for the final state fit (5γ or $\pi^0\gamma\gamma\gamma$) (table 2.3, step 4) as well as for the higher constraint fits (table 2.3, steps 5 and 6). An event was accepted provided that at least one fit of the type $\pi^0 0^-\gamma$ ($0^- = \pi^0$, η, η') succeeded with sufficient probability. The status after the fit on the $\omega\gamma\gamma$-hypothesis is shown in Fig. 2.3. A fit of the full mesonic hypothesis $0^-\omega$ was investigated but finally not used for selection since first it treats the ω meson as stable and secondly one loses control of the background. A consistency check of the applied fits was done instead (see below).
The distributions of the vertices had been determined assuming simple Gaussian shape. This is a very coarse approximation in z-direction. Table 2.4 shows the resulting parameters. These were used in order to reject events from outside the target. The cut on the

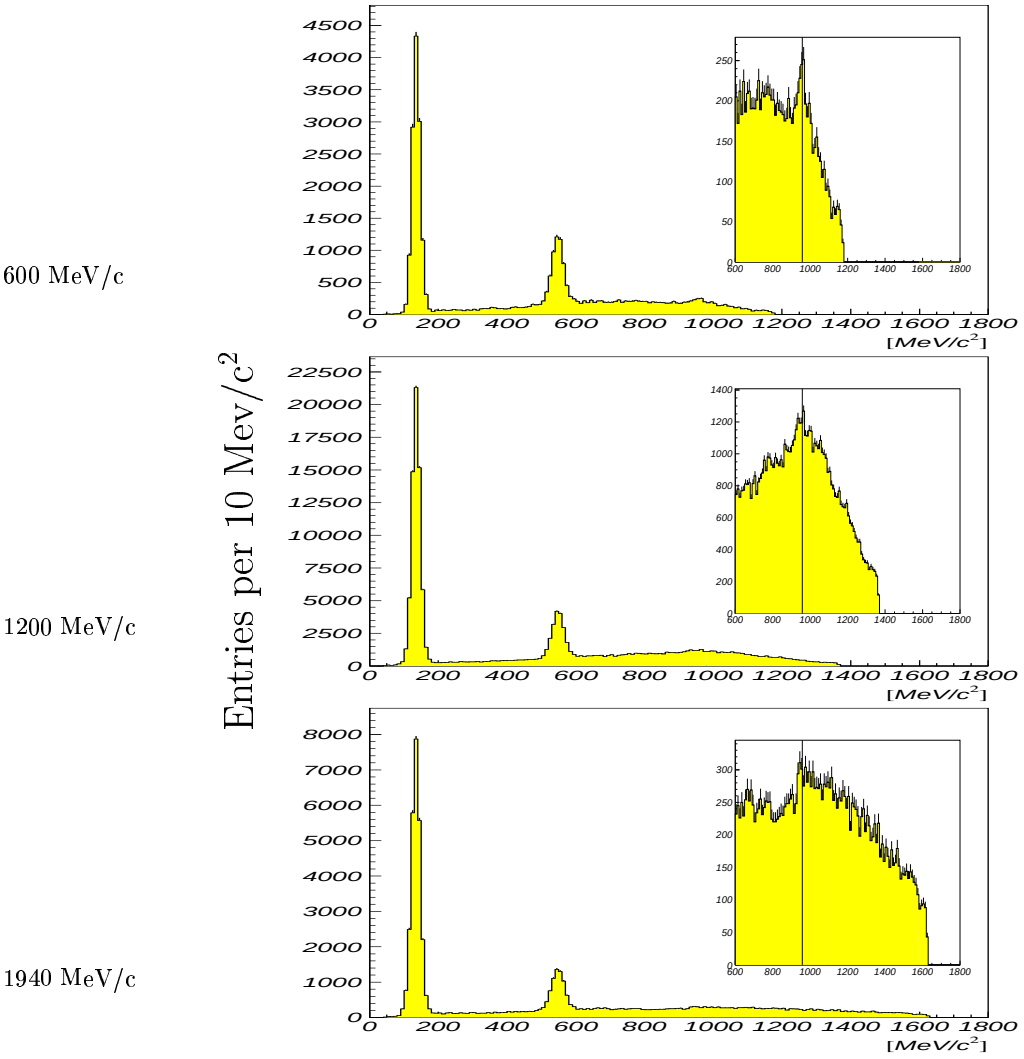

Figure 2.3: *Invariant mass of the $\gamma\gamma$ pair from the $\omega\gamma\gamma$ fit. The π^0 and η mesons are clearly visible. In the detailed part the η' meson appears. The spectra refer to the selection status directly before requiring consistency between the fits. After this requirement only the mesonic structures remain together with the non distinguishable background.*

z component of the vertex is made at 4σ in upstream direction and at 3σ in downstream direction. The tighter cut in downstream direction is made in order to take into account the unsufficient function of the veto counter during the July '92 run period. The cut is done the same way for all run periods in order to be consistent. The distributions for the y and z components of the vertex are very broad. This behaviour is more due to bad convergence of the kinematic fit than to events from outside the target. Therefore windows with 10σ widths are chosen for the cuts on these components in order to save the events for the analysis (table 2.3, step 7).

An event may only be assigned one type, either $\pi^0\omega$ or $\eta\omega$ or $\eta'\omega$. The channels with lower mass mesons are seen much more frequently in the data than the ones with heavier mesons. Therefore there is more background under the heavy meson channels arising from wrong

run period		December 1991	July 1992		April/May 1993		August 1994	
beam momentum [MeV/c]		1200	1200	1940	600	1200	1200	1940
target								
x	μ [cm]	0.210	-0.179	-0.210	-0.149	-0.172	-0.138	-0.152
	σ [cm]	0.974	0.937	0.854	1.040	0.920	0.904	0.849
y	μ [cm]	0.186	0.238	0.086	0.097	0.011	0.078	0.052
	σ [cm]	0.943	0.925	0.855	1.030	0.931	0.963	0.832
z	μ [cm]	0.172	0.771	0.834	0.931	0.840	0.480	0.690
	σ [cm]	1.589	1.575	1.554	1.601	1.553	1.542	1.528
veto counter								
z	μ [cm]	-	11.457		-	-	-	-
	σ [cm]	-	0.973		-	-	-	-

Table 2.4: *Gaussian descriptions of the vertex distributions*

combinatorics of the lighter meson channels than vice versa. For this reason $\pi^0\omega$ events were the first to be selected from the data (table 2.3, step 8), $\eta\omega$ events were selected from the remaining data (table 2.3, step 9) and at last $\eta'\omega$ events are selected from the rest of the data (table 2.3, step 10).
If not requiring convergence of the full hypothesis $0^-\omega$ then at least all considered hypotheses (Table 2.3, steps 5 and 6) have to be consistent. Consistency in that sense means that the assignment of photons to the decay of resonances does not lead to contradictions for the different hypotheses. This method is illustrated in fig. 2.5. There are several possibilities to realize the consistency requirement. Here it was required that the best fits of each hypothesis have to be consistent in the above mentioned sense (table 2.3, steps 8.a, 9.a, 10.a). The selectivity of this method can be seen in fig. 2.4.
Since the kinematic fit was applied on PED basis (either photons or totally merged pions) the thus reconstructed mesons are independent on the mesons recognized by applying the shower mass parametrization on many PED clusters. Therefore it makes sense to require the mesons found by the fit and the mesons found from calorimeter signatures to be consistent. This means that events are rejected if the combinatorics preferred by the fit are not supported by the mesonic signatures in the calorimeter (table 2.3, steps 8.b, 9.b, 10.b).

Further background suppression

Calculating the expected background it turned out that the background contamination was still large, with some sub data samples showing enriched background contaminations. These were the data samples with additional PEDs due to shower fluctuations for all channels (cf. table 2.3, steps 8.c, 9.c, 10.c) and the data samples with totally merged pions for the channels $\eta\omega$ and $\eta'\omega$ (cf. table 2.3, steps 9.d, 10.d). Therefore these sub data samples were rejected.
For the channels of type $\eta\omega$ the main background contributions showed up in small regions of ω decay angle distributions (cf. fig. 2.6.a). After comparing the distributions from Monte Carlo events and the distributions from real data each $\eta\omega$ candidate with a reconstructed

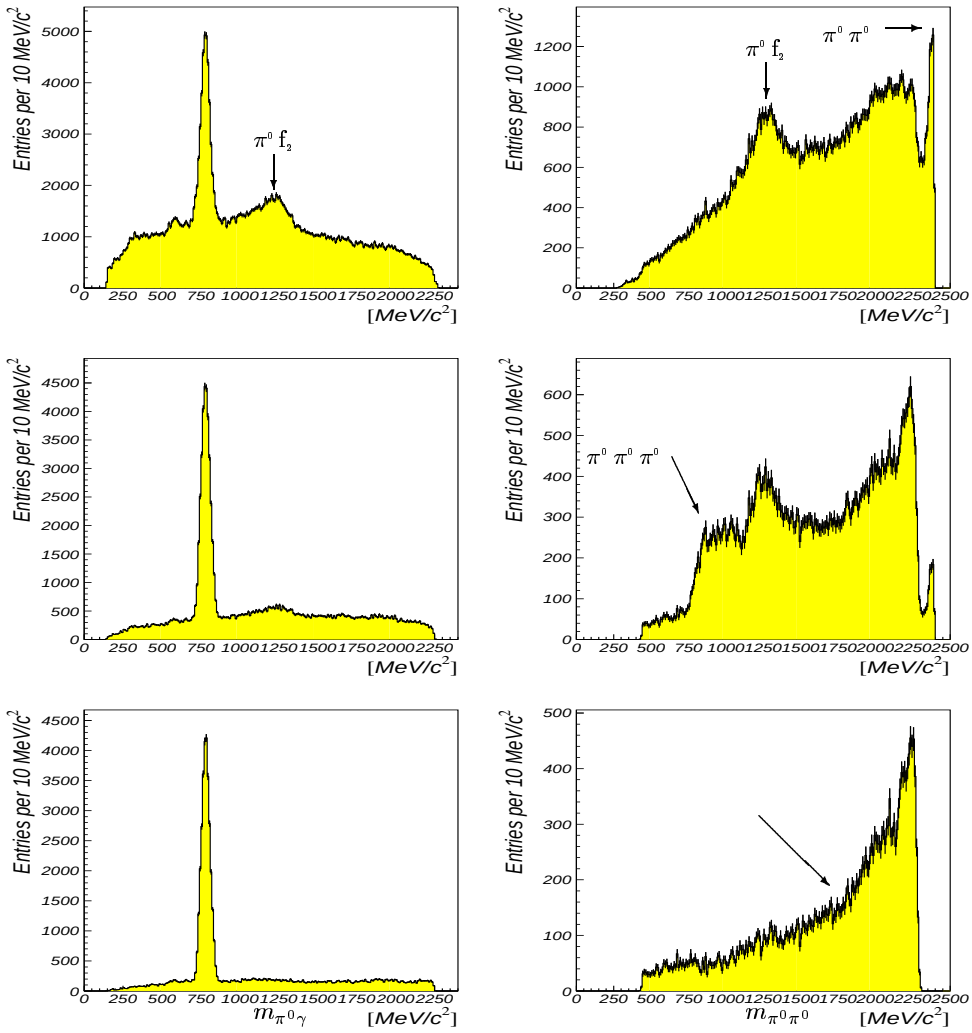

Figure 2.4: *Control spectra for the $0^-\omega$ selection. The chosen example is the channel $\pi^0\omega$ at 1940 MeV/c. The left column shows the invariant mass spectrum of $\pi^0\gamma$ (2 entries per event), the right column shows the invariant mass spectrum of $\pi^0\pi^0$ (1 entry per event). The first line shows the spectra after the $\pi^0\pi^0\gamma$ fit converging, the second line refers to the selection state after all cuts except requiring fit consistency and the third line refers to the state after requiring fit consistency.Clearly visible are background contributions from $\pi^0 f_2$, $\pi^0\pi^0\pi^0{}_{nonresonant}$ and $\pi^0\pi^0$ and their reduction during the selection procedure. An indication for further background contribution is the bend at 1850 MeV/c² in the invariant mass spectrum of $\pi^0\pi^0$ which is not seen in $\pi^0\omega$ Monte Carlo.*

decay angle larger than a certain value was rejected. The values chosen are $\cos(\theta) = 0.84$ for 600 MeV/c, $\cos(\theta) = 0.86$ for 1200 MeV/c and $\cos(\theta) = 0.90$ for 1940 MeV/c (table 2.3, step 9.e).

The channels $\pi^0\omega$ and $\eta\omega$ were selected for all beam momenta. Though the channel $\eta'\omega$ could be observed at all beam momenta the background contamination at the high beam momenta was too large for an analysis. Therefore this channel was only selected for

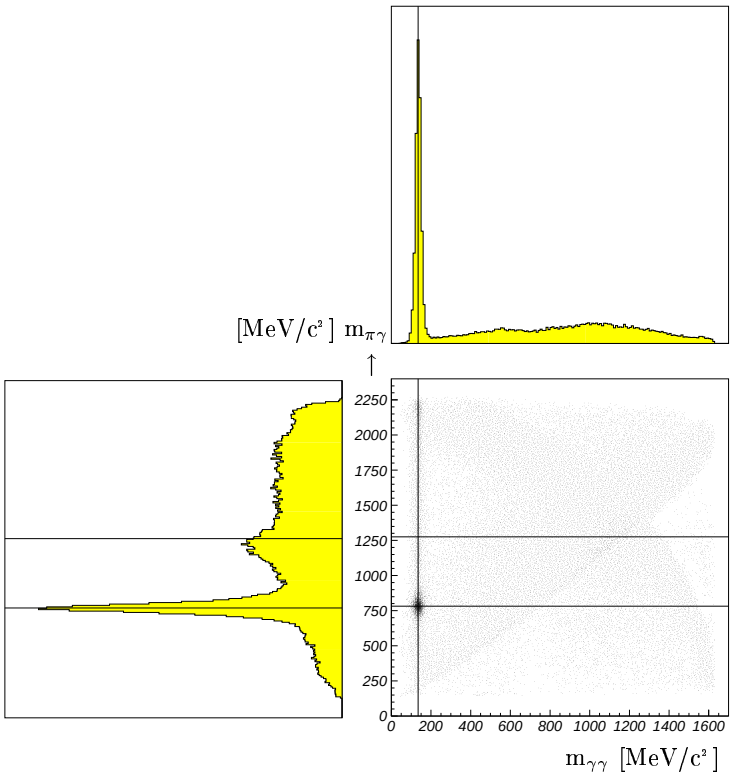

Figure 2.5: *Consistency of $0^-\pi^0\gamma$ and $\omega\gamma\gamma$ fits. The chosen example is data at 1940 MeV/c. The scatter plot shows the invariant masses of $\pi^0\gamma$ from $\pi^0\pi^0\gamma$ (2 entries per event) versus the invariant mass of $\gamma\gamma$ from $\omega\gamma\gamma$. Looking at the invariant mass spectrum of $\pi^0\gamma$ one recognizes, besides the expected ω meson, a background contribution of f_2 (1270) with one low energetic photon from the f_2 decay chain lost. Comparison with the scatter plot reveals that this background is responsible for the broad flat elevation around 1000 MeV/c² in the invariant mass spectrum of $\gamma\gamma$. The latter spectrum dominantly shows the expected π^0 meson. Consistency of both hypotheses is given at the crossing point of the π^0 mass in $\gamma\gamma$ and the ω mass in $\pi^0\gamma$.*

600 MeV/c.

In order to estimate the background within the selected data Monte Carlo data samples of all interesting channels were investigated. In a first step all angular distributions were taken flat as produced by CBGEANT. To improve on that, Monte Carlo data distributed according to the angular distributions found in this analysis and the analysis of the two pseudoscalar channels ($\bar{p}p \longrightarrow 0^-0^-$ [4, 5]) were considered.

An estimate of the contributing background is given in table 2.5. For channels of the type $0^-\omega$ the relative branching ratios and angular distributions from these analyses were used, for channels of type 0^-0^- relative branching ratios and angular distributions from other analyses were used [4, 5].

The main background arises from channels of the types $\bar{p}p \longrightarrow X0^-$ and $\bar{p}p \longrightarrow 0^-0^-0^-$ with $X \longrightarrow 0^-0^-$ and $0^- \longrightarrow \gamma\gamma$. The estimate is based on information from another analysis [15] which at that time was still in progress. For the actual background contribution the final resonance parameters have to be taken into account. Fortunally Monte Carlo studies indicate that in general channels with intermediate resonances ($X0^-$ e.g.) produce

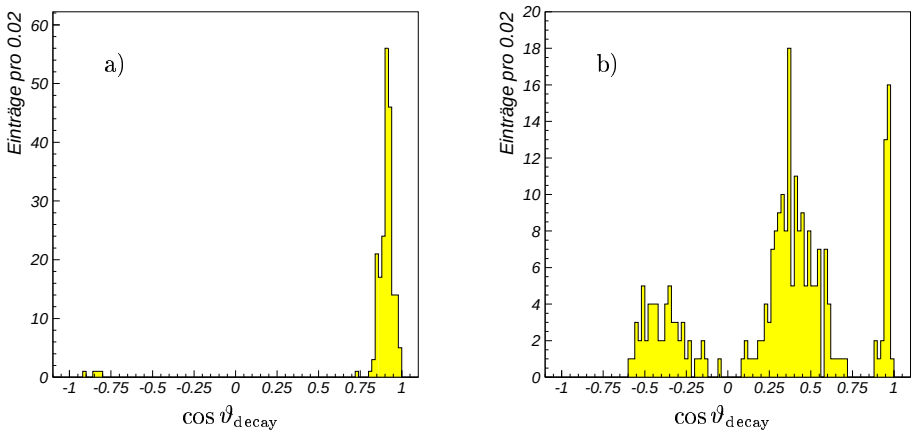

Figure 2.6: *Examples for background behaviour. Fig. a) shows the background in the ω decay angle of the channel $\eta\omega$ at 1940 MeV/c arising from events of the channel $\pi^0\omega$ (Monte Carlo, flat angular distribution). This background may be simply cut off. Fig. b) shows the background in the ω decay angle of the channel $\pi^0\omega$ at 1940 MeV/c arising from events of the channel $\pi^0 f_2(1270)$ (Monte Carlo, flat angular distribution). There is no simple cut for this background and it is hardly analytically describable.*

less background in $\pi^0\omega$ and $\eta\omega$ data than the according mesonic final state ($0^-0^-0^-$ e.g.). Therefore the values given in table 2.5 for the three pseudoscalar channels may be considered as an upper limit. Only the background for 1200 MeV/c shown in table 2.5 is underestimated since no information on the strength of the three pseudoscalar channels were available for this beam momentum.

beam momentum [MeV/c]	600	1200	1940
Total selected statistics			
$\bar{p}p \longrightarrow \pi^0\omega$	8 183	41 663	17 320
background in		$\pi^0\omega$	
from $\pi^0\pi^0$	7.0E-4	1.1E-3	9.4E-4
from $\pi^0\eta$	1.2E-4	1.1E-4	3.8E-3
from $\pi^0\eta'$, $\eta' \longrightarrow \gamma\gamma$	?	$\rightarrow 0.$	9.2E-4
from $\pi^0\eta'$, $\eta' \longrightarrow \omega\gamma$	?	3.9E-5	1.4E-4
from $\eta\eta$	?	$\rightarrow 0.$	2.1E-4
from $\eta\omega$	1.0E-3	7.2E-4	4.2E-4
from $\eta'\omega$	1.9E-4	?	?
from $\pi^0\pi^0\pi^0$	4.7%	?	8.6%
from $\pi^0 f_2$		?	2.4%
from $\pi^0\pi^0\eta$	7.0E-4	?	1.2%
from $\pi^0\eta\eta$	$\rightarrow 0.$	?	$\rightarrow 0.$
from $\eta\eta\eta$	?	?	$\rightarrow 0.$
Total	approx. 5.0%	>> 2.0E-3	approx. 12.9%

beam momentum [MeV/c]	600	1200	1940	600
Total selected statistics				
$\bar{p}p \longrightarrow \eta\omega$	2 880	9 732	3 032	
$\bar{p}p \longrightarrow \eta'\omega$				393
background in		$\eta\omega$		$\eta'\omega$
from $\pi^0\pi^0$	$\rightarrow 0.$	$\rightarrow 0.$	$\rightarrow 0.$	$\rightarrow 0.$
from $\pi^0\eta$	2.5E-4	$\rightarrow 0.$	$\rightarrow 0.$	$\rightarrow 0.$
from $\pi^0\eta'$, $\eta' \longrightarrow \gamma\gamma$	?	1.4E-4	$\rightarrow 0.$	?
from $\pi^0\eta'$, $\eta' \longrightarrow \omega\gamma$	?	6.5E-5	2.2E-4	?
from $\eta\eta$	?	$\rightarrow 0.$	$\rightarrow 0.$	?
from $\pi^0\omega$	2.0%	1.4%	2.1%	6.9%
from $\eta\omega$	-	-	-	7.6%
from $\eta'\omega$	7.1E-4	?	?	-
from $\pi^0\pi^0\pi^0$	1.2%	?	7.9E-3	3.3%
from $\pi^0 f_2$		?	1.4E-3	
from $\pi^0\pi^0\eta$	9.3E-3	?	10.3%	2.9%
from $\pi^0\eta\eta$	3.0E-4	?	2.9E-3	2.7E-3
from $\eta\eta\eta$	?	?	$\rightarrow 0.$	?
Total	approx. 4.2%	>> 1.4%	approx. 13.7%	approx. 20.9%

'?' : background could not be estimated

'$\rightarrow 0.$' : less than 1 background event of this type expected

'$\uparrow$' : the number for $\pi^0\pi^0\pi^0$ includes the number for $\pi^0 f_2$

Table 2.5: *Estimate of the background in the selected data. The total background has to be taken with caution since some background channels (for 1200 MeV/c the most important ones) could not be investigated.*

Chapter 3

Partial wave analysis

A further background reduction was not possible. Also a final description of the background was not possible since the analyses of the main background channels were not finished. Therefore the data were treated as if they were background free.
The experimentally determined angular distributions were described by means of Monte Carlo simulations and theoretical ansatzes. In order to fit the data a maximum likelihood method was used analogous to [16]. In the following the symbol $\mathcal{L}$ is used to denote the negative logarithm of the likelihood.
For annihilation in flight there are three observable angles for the decay chain $\bar{p}p \longrightarrow 0^- \omega \longrightarrow 5\gamma$:

1. the ω production angle,
2. the ω decay angle,
3. the Treiman Yang angle between the two decay planes.

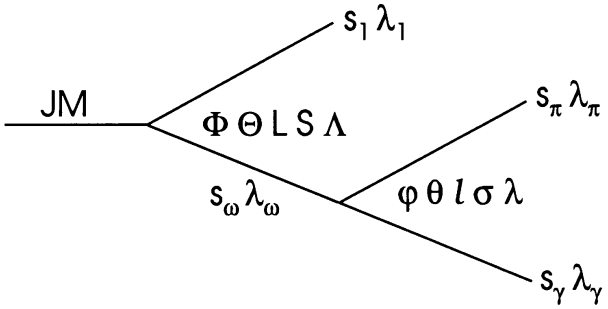

Figure 3.1: *Sketch of the decay $J^M \longrightarrow 0^-\omega \longrightarrow 0^-\pi^0\gamma$. Connected with the decay of the system J^M are the azimuth angle Φ, the polar angle Θ and, for the resulting particles, the orbital angular momentum L, the total spin S and the total helicity Λ. The analogous parameters φ, θ, l, σ and λ belong to the decay of the ω meson.*

	$\bar{p}p$				0^-0^-	$0^-\omega$
J^{PC}	L	S	M	$^{2S+1}L_J$	L (S = 0)	L (S = 1)
0^{--}	not possible from $\bar{p}p$				-	1
0^{-+}	0	0	0	$^1S_0$	-	-
0^{+-}	not possible from $\bar{p}p$				-	-
0^{++}	1	1	0,±1	$^3P_0$	0	-
1^{--}	0	1	0,±1	$^3S_1$	-	1
	2	1	0,±1	$^3D_1$		
1^{-+}	not possible from $\bar{p}p$				1	-
1^{+-}	1	0	0	$^1P_1$	-	0 or 2
1^{++}	1	1	0,±1	$^3P_1$	-	-
2^{--}	2	1	±1	$^3D_2$	-	1 or 3
2^{-+}	2	0	0	$^1D_2$	-	-
2^{+-}	not possible from $\bar{p}p$				-	2
2^{++}	1	1	0,±1	$^3P_2$	2	-
	3	1	0,±1	$^3F_2$		
3^{--}	2	1	0,±1	$^3D_3$	-	3
	4	1	0,±1	$^3G_3$		
3^{-+}	not possible from $\bar{p}p$				3	-
3^{+-}	3	0	0	$^1F_3$	-	2 or 4
3^{++}	3	1	0,±1	$^3F_3$	-	-
even^{--}	J	1	±1		-	J-1 or J+1
even^{-+}	J	0	0		-	-
even^{+-}	not possible from $\bar{p}p$				-	J
even^{++}	J-1	1	0,±1		J	-
	J+1	1	0,±1			
odd^{--}	J-1	1	0,±1		-	J
	J+1	1	0,±1			
odd^{-+}	not possible from $\bar{p}p$				J	-
odd^{+-}	J	0	0		-	J-1 or J+1
odd^{++}	J	1	0,±1		-	-

Table 3.1: *Survey of states for the reactions $\bar{p}p \longrightarrow 0^-\omega$ and (for comparison) $\bar{p}p \longrightarrow 0^-0^-$.*

The full reaction amplitude may be divided into a production part, a decay part and an unknown (maybe resonant) intermediate part. The production amplitude is not explicitly worked out. Selection rules are taken into account by only using allowed transitions for describing the data. It is assumed that the $\bar{p}p$ system is produced in well defined energy and momentum states. Variations of the initial states are assumed to occur in the quantum numbers

- parity (P)
- charge conjugation (C)
- total angular momentum (J)
- z component of the angular momentum (M)

The number of contributing angular momentum states is not known and is determined by the fit procedure. Choosing the beam axis as quantisation axis (z axis) one is able to reduce the 2J+1 possible values of M to only 3 possible values.
The states allowed for the considered decay chain, together with the ones allowed for the final states 0^-0^-, are shown in table 3.1.
A sketch of the considered decay chain denoting the used variables is shown in fig. 3.1.
The amplitude is derived from the formulae given in [9]. In the following parameters causing coherent summation are written as subscripts and parameters causing incoherent summation are written as superscripts of the amplitudes. Then the amplitude reads:

$$\begin{aligned} A_{J\lambda_\omega}^{M\lambda_1\lambda_\pi\lambda_\gamma}(\overline{p}p \to 0^-\omega \to 0^-\pi^0\gamma) = \\ A_{J\lambda_\omega}^{M\lambda_1}(\overline{p}p \to 0^-\omega) \times A_{\lambda_\omega\ (s_\omega=1)}^{\lambda_\pi\lambda_\gamma}(\omega \to \pi^0\gamma) = \\ \sum_{LS} \alpha_{LS}^{(\overline{p}p)}\ (L\ 0\ S\ \Lambda \mid J\ \Lambda)\ (s_\omega\ \lambda_\omega\ s_1\ \lambda_1 \mid S\ \Lambda)\ D_{M\Lambda}^{J\ *}(\Phi,\Theta,0) \times \\ \sum_{l\sigma} \alpha_{l\sigma}^{(\omega)}\ (l\ 0\ \sigma\ \lambda \mid s_\omega\ \lambda)\ (s_\gamma\ \lambda_\gamma\ s_\pi\ \lambda_\pi \mid \sigma\ \lambda)\ D_{\lambda_\omega\lambda}^{s_\omega\ *}(\varphi,\theta,0) \end{aligned} \tag{3.1}$$

The α_{LS} denote the complex spin orbit coupling amplitudes which are used as parameters of the fit. Besides L and S the α_{LS} also depend on M and J as parameters. These indeces are left out for better reading. The observed intensity is given as the absolute square of the amplitude with coherent respectively incoherent summation over all indices of formula 3.1.
Substituting all known particle parameters, using

$$-1 = P(\omega) = P(\gamma)\cdot P(\pi)\cdot(-1)^l = (-1)^l \Rightarrow l \text{ odd} \Rightarrow l = 1 \tag{3.2}$$

and setting

$$\alpha_L := \sqrt{3}\cdot\alpha_{11}^{(\omega)}\cdot\alpha_{L1}^{(\overline{p}p)} \tag{3.3}$$

and splitting up the D functions into their azimuthal and polar parts and taking into account the integration over the non-observable angle Φ when calculating the intensity

$$\int \mid e^{iM\Phi} \mid^2 d\Phi = 2\pi \qquad \forall \qquad M \tag{3.4}$$

one obtains

$$A_{J\lambda_\omega}^{M\lambda_\gamma} = -\sqrt{\pi}\ \lambda_\gamma\ e^{i\lambda_\omega\varphi}\ d_{\lambda_\omega\lambda_\gamma}^1(\cos(\theta))\ d_{M\lambda_\omega}^J(\cos(\Theta))\ \sum_L \alpha_L^{JM}\ (L\ 0\ 1\ \lambda_\omega \mid J\ \lambda_\omega) \tag{3.5}$$

This amplitude is used for describing the data. In the fit routine the complex parameters α_L were taken as two real parameters (length and phase of α_L). The fit was allowed to freely choose each sign. A positive length always may be achieved by redefining the phase. With the α_L's being equal for M = 1 and M = -1 three arbitrary phases remain which were set to zero.
As mentioned before a maximum likelihood method is used in order to fit the theoretical ansatz to the data. Fig. 3.2 and 3.3 show the results of the fit procedure described below in connection with the measured angular distributions.
In order to obtain the maximal contributing angular momenta for each beam momentum several fits with successively increasing maximal angular momentum were performed. For each of these fits every allowed (according to quantum numbers) transition with an angular momentum lower than the assumed maximal one was taken into account. In order

to visualize the result of every step partial intensities were defined. These are intensities calculated for one single angular momentum J and one specification of M as if only this set of parameters contributed. Fig. 3.4 and 3.5 show the development of the partial intensities with successively increasing beam momentum. Also shown is the variation of $\mathcal{L}$. The behaviour of $\mathcal{L}$ is taken as criterion for the determination of the maximal contributing angular momentum. It is assumed that after reaching the maximal contributing angular momentum (and therefore the best fit), the change in the likelihood with each step levels off and comes closer to the curve which is expected for the added parameters only describing statistical fluctuations (cf. the open rhombuses in fig. 3.4 and 3.5).
From this fit procedure the maximal contributing angular momenta turn out to be

- $J_{max} = 5$ for $\bar{p}p \longrightarrow \pi^0\omega$ at 1940 MeV/c
- $J_{max} = 5$ for $\bar{p}p \longrightarrow \eta\omega$ at 1940 MeV/c
- $J_{max} = 4$ for $\bar{p}p \longrightarrow \pi^0\omega$ at 1200 MeV/c
- $J_{max} = 3$ for $\bar{p}p \longrightarrow \eta\omega$ at 1200 MeV/c
- $J_{max} = 3$ for $\bar{p}p \longrightarrow \pi^0\omega$ at 600 MeV/c
- $J_{max} = 3$ for $\bar{p}p \longrightarrow \eta\omega$ at 600 MeV/c
- J_{max} compatible with 3 for $\bar{p}p \longrightarrow \eta'\omega$ at 600 MeV/c

Some tendencies are observed:

- even angular momenta are suppressed for all channels
- the maximal angular momenta also are the dominant ones for $\bar{p}p \longrightarrow \pi^0\omega$
- the maximal angular momenta are larger than the dominant ones for $\bar{p}p \longrightarrow \eta\omega$
- (M = 0) singlet states are preferred for $\bar{p}p \longrightarrow \pi^0\omega$
- (M = 0) triplet states are preferred for $\bar{p}p \longrightarrow \eta\omega$ (exception: 1200 MeV/c).

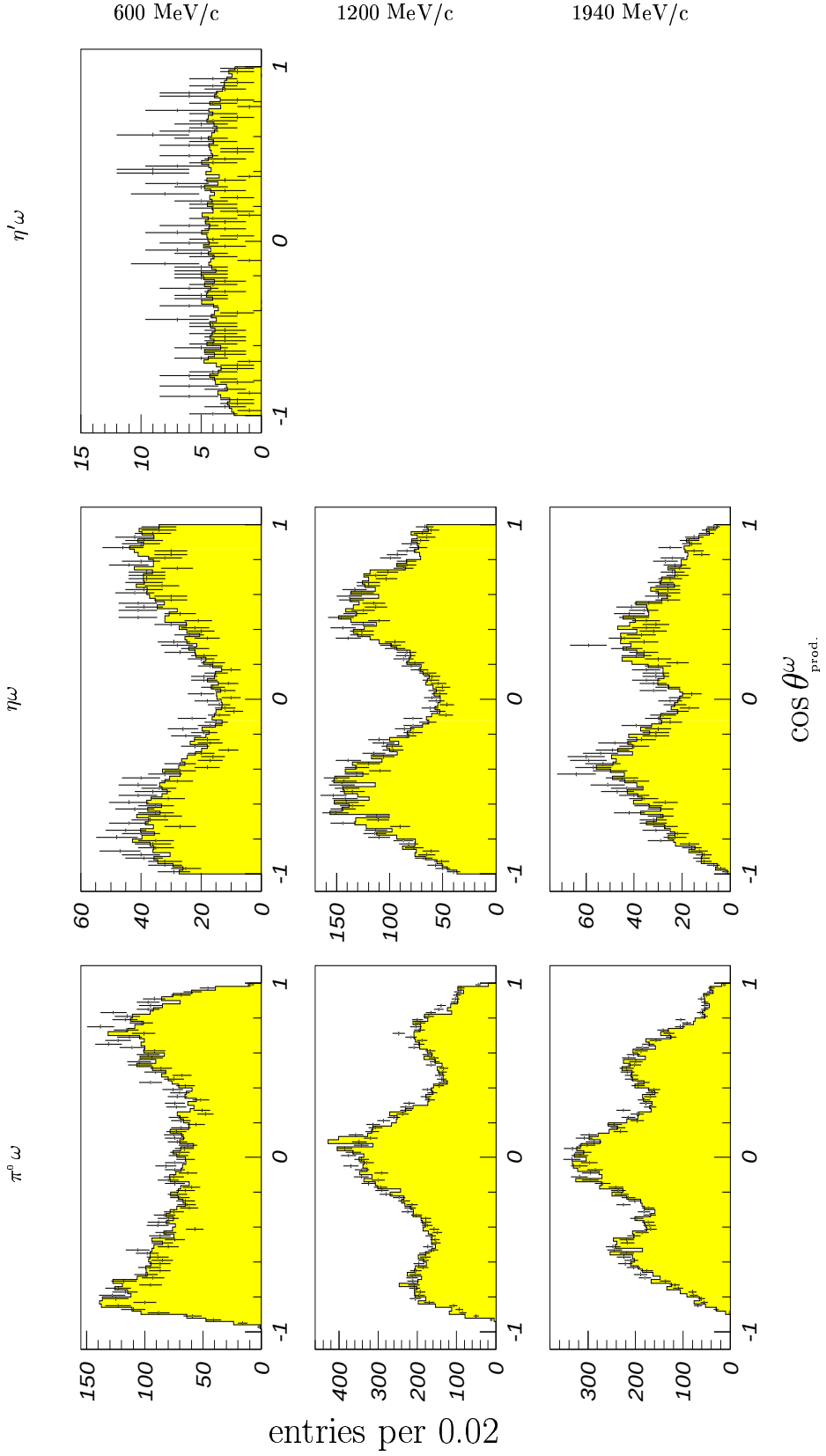

Figure 3.2: *Distributions of the ω production angle (not corrected for acceptance). The data show error bars, the shaded areas indicate the fit results.*

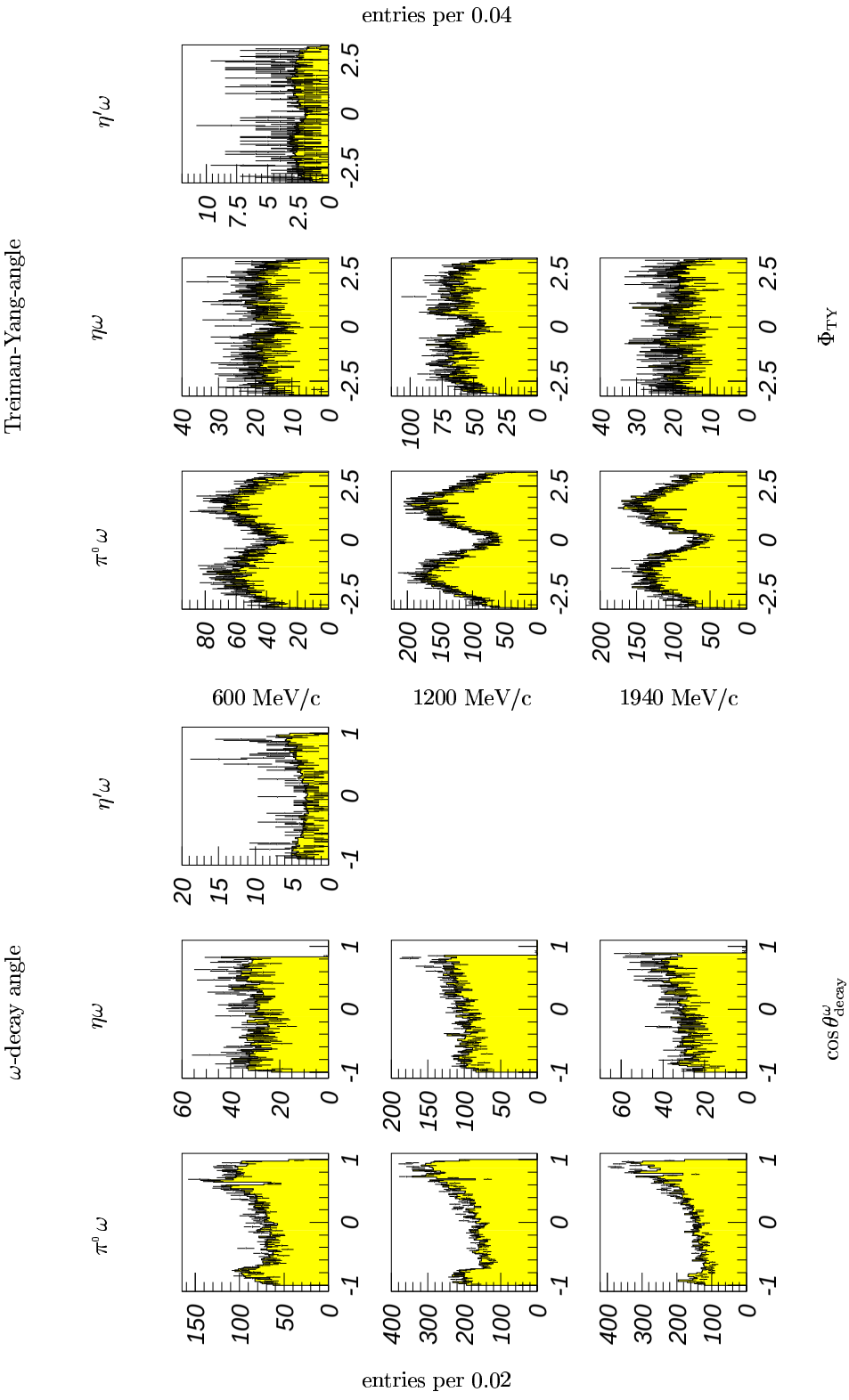

Figure 3.3: *Distributions of the ω decay angle and the Treiman Yang angle (not corrected for acceptance). The data show error bars, the shaded areas indicate the fit results.*

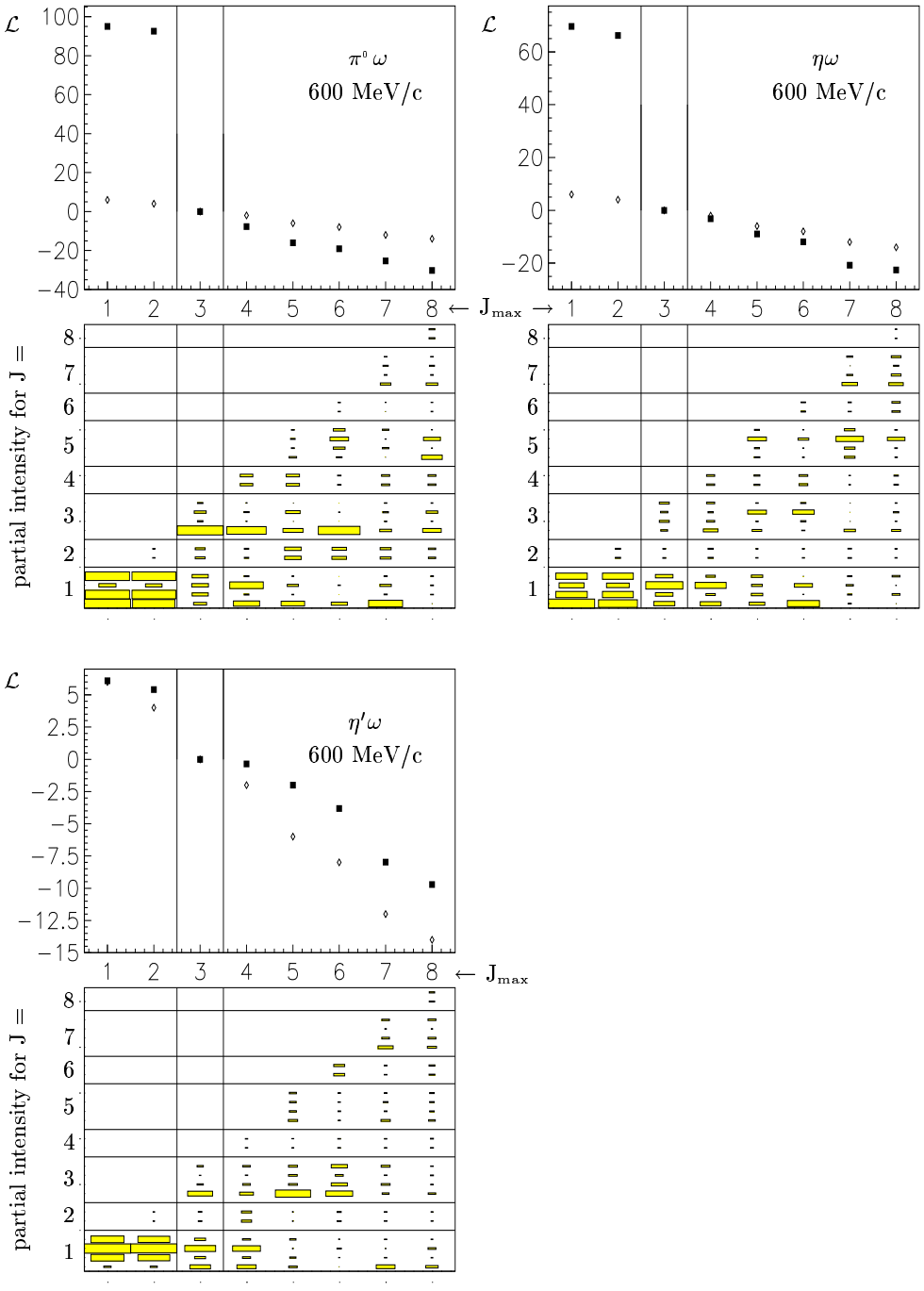

Figure 3.4: *Development of $\mathcal{L}$ (black squares), relative to the "best fit" (selected column), and the partial intensities with increasing J_{max}. The order of the partial intensities is from top to bottom: singlet M = -1,0,+1 for J odd and triplet M = -1,+1 for J even.*

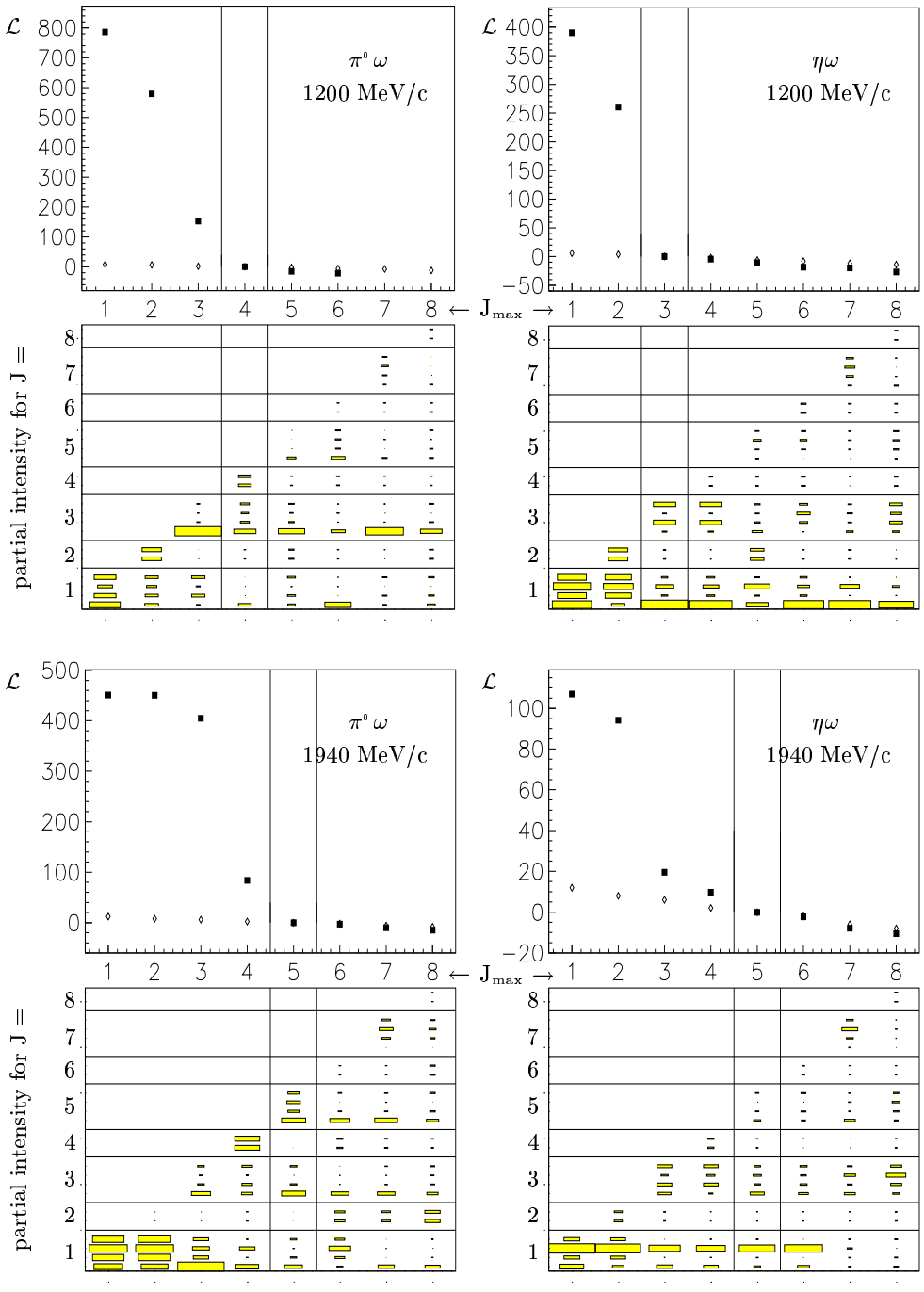

Figure 3.5: *Development of $\mathcal{L}$ (black squares), relative to the "best fit" (selected column), and the partial intensities with increasing J_{max}. The order of the partial intensities is from top to bottom according to (singlet M = 0, triplet M = -1,0,+1) for J odd and (triplet M = -1,+1) for J even.*

In order to obtain the originally produced angular distributions one usually performs a correction for acceptance. Due to the vanishing acceptance near the beam axis this is not possible for some channels. Therefore Monte Carlo simulated data samples were weighted according to the obtained angular distributions in order to visualize the original spectra. This was done consistently for all $0^-\omega$ channels as well as for the 0^-0^- channels [4, 5] which are interesting to compare to the $0^-\omega$ channels. These angular distributions are shown in fig. 3.6 and 3.7. Interesting points are

- the similarity of the distributions of the production angle for $\pi^0\pi^0$ and $\pi^0\omega$,
- the similarity of the distributions of the production angle for $\eta\eta$ and $\eta\omega$,
- the small variation of the distributions of the ω decay angle for all $0^-\omega$ channls,
- the complementary behaviour of the Treiman Yang angle for $\pi^0\omega$ and $\eta\omega$.

decay channel		$\pi^0\pi^0$	$\pi^0\eta$	$\pi^0\omega$	$\eta\eta$	$\eta\omega$	$\omega\omega$	$\eta'\omega$
mass [MeV/c^2]		269.95	682.43	916.92	1094.90	1329.39	1563.88	1739.71
momentum	600 MeV/c	2		3		3		3
	1200 MeV/c	4	4	4	4	3		
	1940 MeV/c	6	6	5	4	5	4	

Table 3.2: *Contributing maximal angular momenta for $0^-\omega$, 0^-0^- [4, 5] and $\omega\omega$ [10]*

It is interesting to consider the dependence of the maximal contributing angular momenta on the produced mass. Tab. 3.2 shows a slight tendency in the channels $\pi^0\omega$ and $\eta\omega$ at 1200 MeV/c of a lower maximal angular momentum with higher produced mass. This tendency is supported by the results from the other channels 0^-0^- [4, 5] and $\omega\omega$ [10]. Comparing some 0^-0^- channels with some $0^-\omega$ channels at the same momentum one finds the lighter 0^-0^- channel to show a lower maximal angular momentum than the heavier $0^-\omega$ channel. This observation does not contradict the above mentioned tendency since according to their quantum numbers 0^-0^- channels may not be produced from odd angular momentum states.
Besides the partial wave contents the relative branching ratios of the observed channels are interesting. Again the $0^-\omega$ channels are compared with the results from the 0^-0^- channel analyses [4, 5]. With the observed reaction rates, the known branching ratios [19]

$$BR(\omega \to \pi^0\gamma) = (8.5 \pm 0.5)\% \quad (3.6)$$
$$BR(\pi^0 \to \gamma\gamma) = (98.798 \pm 0.032)\% \quad (3.7)$$
$$BR(\eta \to \gamma\gamma) = (38.8 \pm 0.5)\% \quad (3.8)$$
$$BR(\eta' \to \gamma\gamma) = (2.12 \pm 0.13)\% \quad (3.9)$$

and assuming a negligible background contamination one obtains the relative branching ratios shown in table 3.3. For the calculation of these relative branching ratios the non-flat efficiencies of the mesonic production angles were taken into account. In order to compare the results with annihilation at rest the corresponding numbers from [17] are also included in table 3.3.

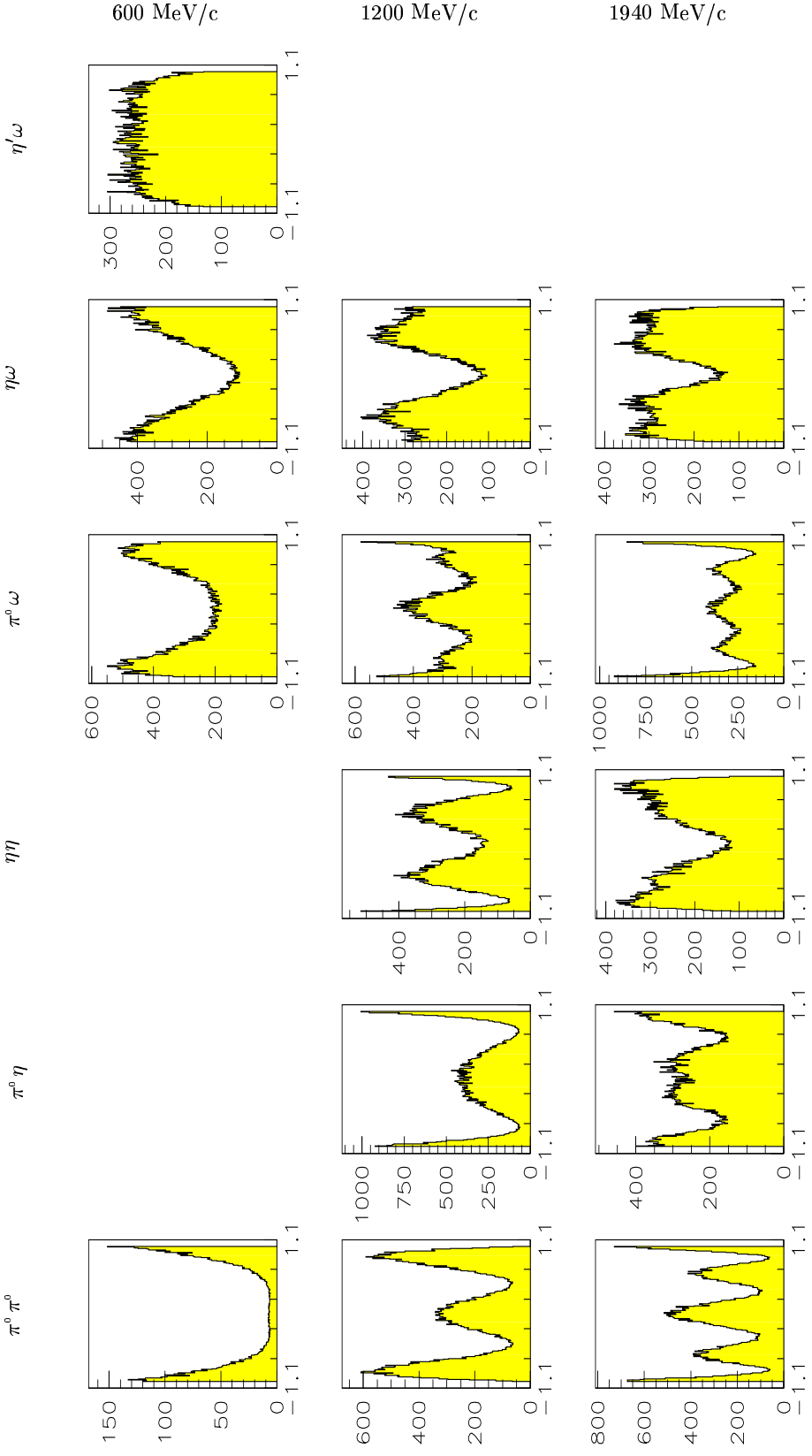

Figure 3.6: *Monte Carlo data samples distributed according to the obtained angular distributions. The number of entries (in arbitrary units) is plotted against the cosine of the production angle.*

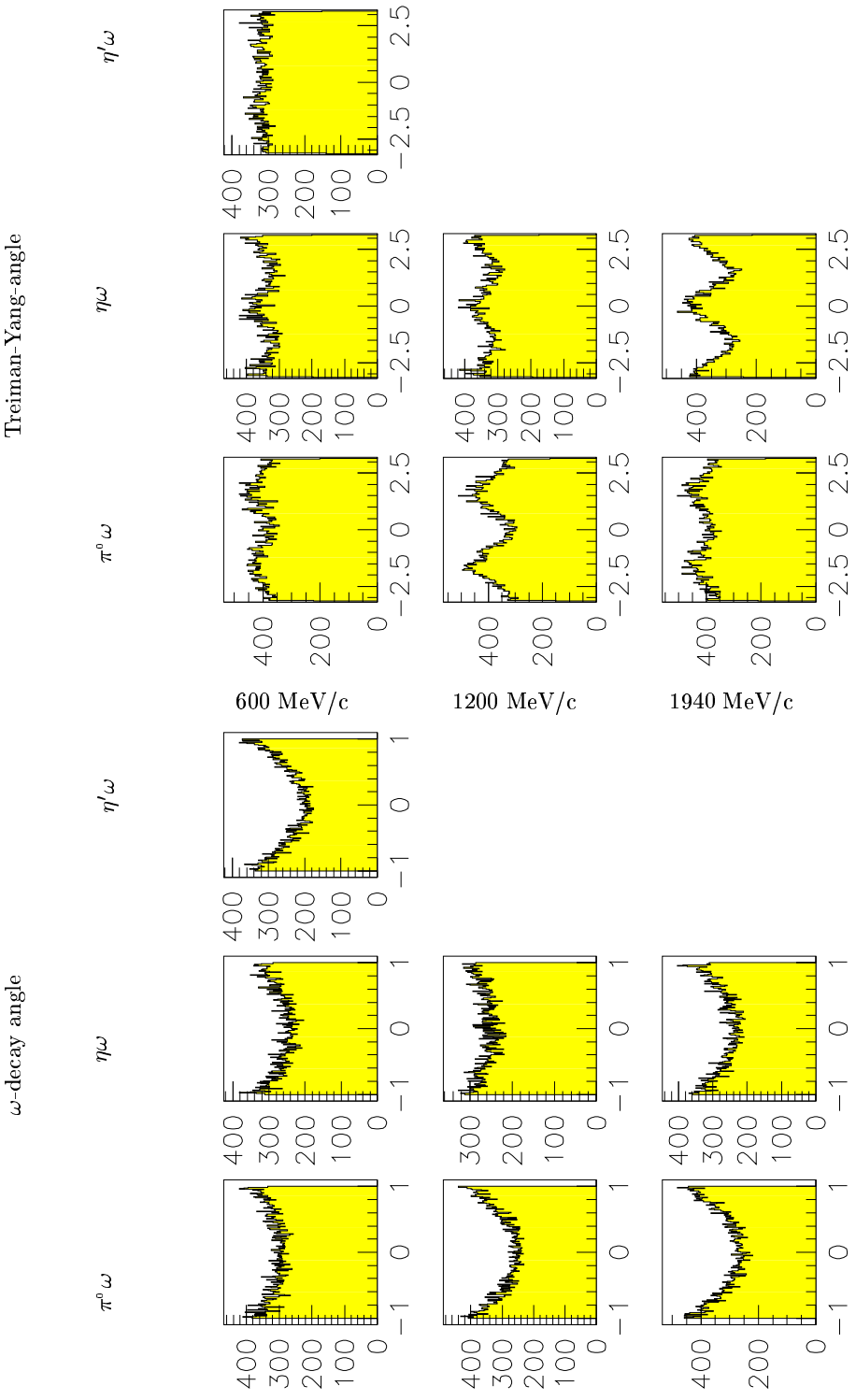

Figure 3.7: *Monte Carlo data samples distributed according to the obtained angular distributions. The number of entries (in arbitrary units) is plotted against the cosine of the ω decay angle or the Treiman Yang angle in radiants respectively.*

beam momentum [MeV/c]	at rest	600	1200	1940
$\frac{\overline{p}p\to\pi^0\omega}{\overline{p}p\to\pi^0\pi^0}$	8.3 ± 0.8	7.7 ± 0.7	5.6 ± 0.4	5.4 ± 0.4
$\frac{\overline{p}p\to\pi^0\omega}{\overline{p}p\to\pi^0\eta}$	27.0 ± 2.7	14.6 ± 2.2	8.8 ± 0.6	5.0 ± 0.3
$\frac{\overline{p}p\to\eta\omega}{\overline{p}p\to\pi^0\eta}$	71.2 ± 6.9	12.8 ± 2.0	5.9 ± 0.4	2.7 ± 0.2
$\frac{\overline{p}p\to\pi^0\omega}{\overline{p}p\to\pi^0\eta'}$	46.6 ± 6.2	?	5.3 ± 0.5	2.3 ± 0.2
$\frac{\overline{p}p\to\eta\omega}{\overline{p}p\to\eta\eta}$	92.1 ± 9.2	?	18.2 ± 1.3	5.7 ± 0.4
$\frac{\overline{p}p\to\eta\omega}{\overline{p}p\to\pi^0\omega}$	2.6 ± 0.3	0.9 ± 0.1	0.7 ± 0.1	0.6 ± 0.1
$\frac{\overline{p}p\to\eta'\omega}{\overline{p}p\to\pi^0\omega}$	1.4 ± 0.2	1.9 ± 0.2	?	?
$\frac{\overline{p}p\to\eta'\omega}{\overline{p}p\to\eta\omega}$	0.5 ± 0.1	2.2 ± 0.3	?	?

Table 3.3: *Summary of the obtained relative branching ratios.*

Bibliography

[1] Application Software Group, CERN: *HBOOK*, CERN program library long writeup Y250, unpublished

[2] Application Software Group, CERN: *MINUIT - Function minimization and error analysis*, CERN program library long writeup D506, unpublished

[3] K. Beuchert, M. Kunze, J. Lüdemann, K. Peters, J. Salk: *CBoOff - Offline analysis for C-programmers*, CB-note 166, unpublished

[4] K. Beuchert: *Untersuchungen zur $\bar{p}p$-Annihilation im Fluge am Crystal-Barrel-Detektor*, PhD thesis, Ruhr-Universität Bochum, 1995

[5] K. Beuchert: *Analysis of $\bar{p}p \longrightarrow 0^-0^-$ in flight*, technical report, in preparation

[6] R. Brun, F. Bruyant, M. Maire, A. C. McPherson, P. Zanarini: *GEANT*, CERN DD/EE/84-1

[7] R. Brun, O. Couet, C. Vandoni, P. Zanarini: *PAW*, CERN program library long write-up Q121, unpublished

[8] M. Burchell, M. Doser: *Global tracking particle bank structure*, CB-note 118, unpublished

[9] S. U. Chung: *Spin formalisms*, CERN 71-8, 1971

[10] V. Credé: *Untersuchung der Produktion von $\omega\omega$-Mesonen in der Antiproton-Proton-Annihilation im Fluge*, diploma thesis, Bochum, May 1996, unpublished

[11] T. Degener: *Untersuchung elektromagnetischer Schauer im Crystal Barrel Kalorimeter mit k"unstlichen neuronalen Netzen*, diploma thesis, Bochum August 1993, unpublished

[12] G. Folger, M. Doser: *Offline reconstruction software*, CB-note 121, unpublished

[13] F.-H. Heisius, T. Kiel, P. Schmidt: *Crystal data reconstruction software*, CB-note 92, unpublished

[14] P. Hidas, G. Pinter: *Kinematic fitting software*, CB-note 138, unpublished

[15] J. Lüdemann: *Beobachtung von Resonanzen in der Proton-Antiproton-Annihilation im Fluge in drei pseudoskalare Mesonen*, PhD thesis, Ruhr-Universität Bochum, 1995

[16] J. Lüdemann: *Log likelihood*, CB-note 261, unpublished

[17] M. Merkel: *Proton-Antiproton-Vernichtung in Ruhe in $\pi^0 X$, ηX und ωX mit $X = \pi^0$, η und η'*, PhD thesis, Mainz 1993

[18] C. A. Meyer: *Chamber reconstruction software - Locater*, CB-note 93, unpublished

[19] Particle Data Group (M. Aguilar-Benitez et al.): *Review of particle properties*, Phys Rev. D50 (1994) 1173

[20] K. Peters: *The Monte Carlo programmer's guide for the LEAR Crystal Barrel*, CB-note 103, unpublished

[21] P. Schmidt: *Pi0 reconstruction and optional fitting software (PI0FND)*, CB note 133, unpublished